Video-based Human-Object Interaction Detection from Tubelet Tokens

Anonymous Author(s)

Abstract

We present a novel vision Transformer, named TUTOR, which is able to learn tubelet tokens, served as highly-abstracted spatiotemporal representations, for video-based human-object interaction (V-HOI) detection. The tubelet tokens structurize videos by agglomerating and linking semantically-related patch tokens along spatial and temporal domains, which enjoy two benefits: 1) Compactness: each tubelet token is learned by a selective attention mechanism to reduce redundant spatial dependencies from others; 2) Expressiveness: each tubelet token is enabled to align with a semantic instance, *i.e.*, an object or a human, across frames, thanks to agglomeration and linking. The effectiveness and efficiency of TUTOR are verified by extensive experiments. Results show our method outperforms existing works by large margins, with a relative mAP gain of 16.14% on VidHOI and a 2 points gain on CAD-120 as well as a $4\times$ speedup.

1 Introduction

Human-object interaction (HOI) detection is a detailed scene understanding task, which requires both localization of interacted human-object pairs and recognition of interaction labels. Existing methods mostly investigated detecting HOIs in static images without capturing temporal information (Figure 1 (a)), thus lack the ability to detect time-related interactions (*e.g.*, `shoot` or `pass` a basketball). However, interactions are more of time-related in practical scenario, leading to a strong demand to detect HOIs from videos, a more challenging problem built on spatiotemporal semantic representations.

Transformer, originated from natural language processing (NLP), is an intuitive choice for its eminent capability of reasoning long-range dependencies, in which one of the most crucial components is the token. A token serves as an element of data representations, which is usually a word in language. However, unlike language that naturally has such a discrete signal space for building tokenized dictionaries, images lie in a continuous and high-dimensional space. To address this issue, vision Transformer (ViT) [7] provided a solution that divides each image into several local patch tokens ("visual words") to structurize the entire image as a "visual sentence"(Figure 1(b)). This solution has become a *de facto* tokenization standard followed by most existing Transformer-based methods, which has achieved excellent performance for various vision tasks, especially image classification.

Nevertheless, this patch based tokenization strategy might not be proper for video-based HOI (V-HOI) detection (as the performance degradation of the ViT-like framework shown in Table. 1a). We find that the reason is the patch tokens generated by regular splitting are difficult to exactly capture instance-level semantics (an instance is an object or a human, *e.g.*, the basketball shooter in Figure 1), which yet is crucial for V-HOI detection to reason the interaction labels. These patch tokens inevitably suffer from redundancy due to an information mixture from different instances as well as insufficiency due to only a part occupancy of an instance, which limit their representation ability.

Submitted to 36th Conference on Neural Information Processing Systems (NeurIPS 2022). Do not distribute.

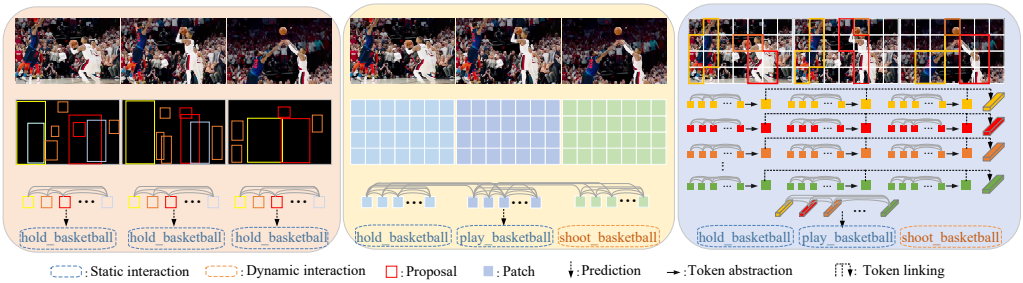

(a) proposals (b) patch tokens (c) tubelet tokens

Figure 1: Illustration of different strategies for V-HOI detection, which are built on different representations. (a) Image-based HOI detection methods, which process each frame as *i.i.d* data, and recognize the interrelations among pre-detected proposals in each frame independently. (b) ViT-like V-HOI detection frameworks, which perform global attention mechanism on patch tokens over space and time. (c) Our proposed TUTOR, which structurizes a video into a few tubelet tokens by token abstraction along spatial domain and token linking along temporal domain.

In this paper, we present TUTOR, a new Transforme**R** for V-HOI detection built on **TU**belet **TO**kens, handling aforementioned limitations favorably. The tokenization of the tubelet tokens is not based on fixed regular splitting but is jointly performed with the learning of the Transformer encoder. This enables the tubelet tokens to progressively emerge and represent high-level visual semantics. Concretely, first, along the spatial domain, we alternatively update the representation for each patch token by a selective attention mechanism and agglomerate semantically-related patch tokens into instance tokens. The selective attention mechanism ensures that attention is performed among tokens expected to belong to the same instance, which reduces redundant spatial dependencies from others. Then, along the temporal domain, we link instance tokens across frames to form the tubelet tokens. Figure 1(c) illustrates the process of tubelet token generation. Experimental results show that TUTOR outperforms existing sota methods by large margins. Specifically, we achieve a relative mAP gain of 16.4% on VidHOI [5] and a 2 points F1 score gain on CAD-120 [22], with a $4\times$ inference speedup.

2 Related Work

HOI detection. Most previous works are devoted to detecting HOIs in static images [3, 10, 11, 13, 14, 16, 19, 21, 23, 24, 27, 29, 35, 38, 40, 41, 43, 45, 46, 49, 50, 51, 37, 53, 20, 4, 47]. Without considering temporal information, these methods fail to detect time-related interactions, restricting their value in practical applications. In contrast, video-based HOI detection is a more practical problem, which however is less explored [35, 33, 34, 36, 5, 42, 18]. [35, 36, 42] detected HOIs in videos by building graph neural networks to capture spatiotemporal information. In [33], HOI "hotspots" can be directly learned from videos by jointly training a video-based action recognition network as well as an anticipation model. Inspired by image-based methods, [5] introduced a two-stage framework where the frame-wise human/object features are firstly extracted by using trajectories, and then HOIs are detected by processing the instance features as well as auxiliary features, including spatial configurations and human poses. However, these methods lack the ability to model long range contextural information, resulting in poor performance when the interacted human and object are far apart. [18] proposed a spatiotemporal Transformer to reason human-object relationships in videos, which detects human/object proposals firstly and then captures spatial and temporal information by using two dense-connected Transformers, respectively. However, such dense-connected manner introduces extra computation and ambiguity in token representation.

Transformer in video analysis. Transformer [39] has shown a great potential in video analysis, *e.g.*, action recognition [28, 48], video restoration [25], video question answering [12], video instance segmentation [44] and etc. However, most spatiotemporal Transformer follow the *de facto* scheme of ViT [7], *i.e.*, simply dividing an image into local patches and stacking global attention, which lacks sufficient exploration of the properties of visual signal, thus suffering from insufficiency token representation and explosive computation.

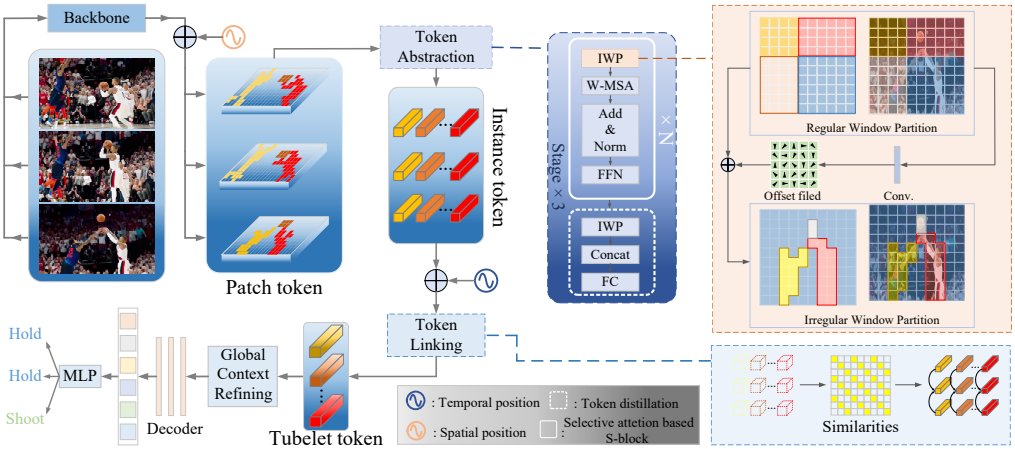

Figure 2: **The architecture of TUTOR.** It consists of 1) a backbone to generate the initial patch tokens; 2) a token abstraction module that alternatively update token representations and agglomerate patch tokens, to progressively form instance tokens; 3) a token linking module that links the semantically related instance tokens across different frames to form tubelet tokens; 4) a simple global attention layer to reinforce the global contextual information and 5) a standard Transformer decoder to decode the HOI instances. We use different dashed squares to zoom in on different key modules.

3 Methodology

The main idea of TUTOR is to structurize a video into a few tubelet tokens, which serve as highly-abstracted spatiotemporal representations. To this end, we propose a reinforced tokenization strategy, which jointly performs tokenization and optimization of the Transformer encoder, as illustrated in Figure 2. The process of tubelet token generation consists of two steps: 1) Token abstraction along the spatial domain, where patch tokens are alternatively updated by a selective attention mechanism and agglomerated into instance tokens; 2) Token linking along the temporal domain, where instance tokens across frames are linked to form tubelet tokens. We describe these two steps in details below.

3.1 Backbone

Taking a video clip $\mathbf{x} \in \mathbb{R}^{T\times H\times W\times 3}$ that consists of T frames with size $H \times W$ as the input, we use a ResNet [15] followed by a feature pyramid network (FPN) [26] as the backbone on t-th frame to generate a feature map $\mathbf{z}_{(t,b)} \in \mathbb{R}^{\frac{H}{4}\times\frac{W}{4}\times C_0}$, where $t = 1, 2, .., T$ and $C_0 = 32$ is the channel number of the initial feature map.

3.2 Token Abstraction

Token abstraction is organized in 3 *Stages* through a hierarchy of Transformer layers. Each stage performs token representation learning by a selective attention mechanism and merges semantically-related patch tokens into instance tokens by an agglomeration layer. Here, we denote the feature map of t-th frame inputted into s-th stage as $\mathbf{z}_{(t,s)} \in \mathbb{R}^{H_s\times W_s\times C_s}$. Specifically, $\mathbf{z}_{(t,1)} = \mathbf{z}_{(t,b)}$.

Selective attention. To eliminate the redundancy caused by information mixture from different instances, we are motivated to selectively calculate attention weights among related tokens, *i.e.*, tokens belong to the same instances. To this end, we propose an irregular window partition (IWP) mechanism (orange rectangle in the right of Figure 2), a simple yet effective strategy that samples a group of related tokens into a local window. IWP is inspired from regular window partition [30], where the tokens are grouped by sliding a regular rectangle $\mathcal{R}$ with size of $S_w \times S_w$ over the feature map $\mathbf{z}_{(t,s)}$ in s-th stage. For instance, $\mathcal{R} = \{[0, 0], [0, 1], ..., [3, 4], [4, 4]\}$ defines a regular window with size of 5×5. Then, for the i-th regular window, we have

$$\mathcal{Z}^i_{\text{rw}} = \{\mathbf{z}_{(t,s)}(\mathbf{p}_n + [x^i_w, y^i_w]) \mid \mathbf{p}_n \in \mathcal{R}\}, \tag{1}$$

where $\mathbf{z}_{(t,s)}([x,y]) \in \mathbb{R}^{1\times C_s}$ denotes the feature vector at spatial location $[x,y]$ and $[x_w^i, y_w^i]$ is the location of the top-left point of i-th window. However, as shown in Figure 2, regular windows can easily divide an instance into several parts due to the limitation of a fixed shape, leads to unrelated tokens within a window, *i.e.*, belonging to different instances. Inspired by deformable DETR [52] and deformalbe convolution [6], (the detailed comparison is described in Appendix) IWP makes a simple change by augmenting regular grid $\mathcal{R}$ with learned offsets, which allows the generated irregular windows to be aligned with humans/objects with arbitrary shapes. With offsets $\{\Delta\mathbf{p}_n | n = 1, 2, ..., N\}$ and $N = |\mathcal{R}|$, for the tokens in i-th irregular window, we have

$$\mathcal{Z}_{\text{irw}}^i = \{\mathbf{z}_{(t,s)}(\mathbf{p}_n + [x_w^i, y_w^i] + \Delta\mathbf{p}_n) \mid \mathbf{p}_n \in \mathcal{R}\}. \tag{2}$$

Specifically, $\Delta\mathbf{p}_n$ are learned by performing a convolutional layer with kernel size of 3×3 over the input feature map $\mathbf{z}_{(t,s)}$. As the offsets are typically fractional, the right part of Eq. 2 is implemented practically via bilinear interpolation as

$$\mathbf{z}_{(t,s)}(\mathbf{p}) = \sum_{\mathbf{q}} \mathrm{B}(\mathbf{q}, \mathbf{p}) \cdot \mathbf{z}_{(t,s)}(\mathbf{q}), \tag{3}$$

where $\mathbf{p} = \mathbf{p}_n + [x_w^i, y_w^i] + \Delta\mathbf{p}_n$ denotes an arbitrary location, $\mathbf{q}$ enumerates all neighboring integral locations, and B is the bilinear interpolation kernel.

On this basis, we alternatively update the token representation by stacking several *S-blocks* (rectangle in white solid line in Figure 2) that are built on selective attention, *i.e.*, performing attention mechanism within irregular windows. Specifically, each block is computed as

$$\hat{\mathbf{z}}_{\text{irw}}^l = \text{IWP}(\mathbf{z}^{l-1}, S_w), \tag{4}$$

$$\hat{\mathbf{z}}^l = \text{W-MSA}(\text{LN}(\hat{\mathbf{z}}_{\text{irw}}^l + \mathbf{p}_e^l)) + \text{Flatten}(\mathbf{z}^{l-1}), \tag{5}$$

$$\mathbf{z}^l = \text{Reshape}(\text{MLP}(\text{LN}(\hat{\mathbf{z}}^l)) + \hat{\mathbf{z}}^l), \tag{6}$$

where $\mathbf{z}^l$ is updated representation for all tokens, $\mathbf{p}_e^l$ is sine-based spatial position encoding at l-th *S-block*, and $\hat{\mathbf{z}}$ denotes various intermediate features. Here, we factorize the conventional 3D position encoding into a 2D spatial position encoding and a 1D temporal one since the spatial and temporal information are separately extracted. In detail, "W-MSA" denotes window-based multi-head self-attention, "LN" is layer normalization and "MLP" refers to multi-layer perceptron. Since the convolution layer in IWP is operated on 2D feature map yet attention is calculated on sequential features, we use a "Flatten" ($2D \rightarrow 1D$) operation to collapse the spatial dimension and a "Reshape" ($1D \rightarrow 2D$) operation to restore it. The computational complexity of a global MSA (G-MSA) block and an irregular-window-based block (IW-MSA) for total T frames at s-th stage are respectively:

$$\Omega(\text{G-MSA}) = 4H_sW_sTC_s^2 + 2(H_sW_sT)^2C_s, \tag{7}$$

$$\Omega(\text{IW-MSA}) = 4H_sW_sTC_s^2 + 2(S_w^2 + K^2)H_sW_sTC_s, \tag{8}$$

where $K = 3$ is the kernel size of convolutional layer and S_w is fixed as 7. In comparison, IW-MSA can effectively reduce the computational complexity. In our experiment, the number of *S-block* for (1-3)-th stage is set to 1, 1, 3, respectively.

Token agglomeration. We perform token agglomeration at the end of each stage to merge semantically similar tokens. Specifically, we first perform IWP with a window size of 2×2 to dynamically sample every 4 related tokens into a window. Then, we concatenate the tokens within each window and apply a fully-connected (FC) layer on the concatenated $4C_s$-dimensional features. We set the output dimension to $2C_s$. It reduces the number of tokens by a multiple of $2 \times 2 = 4$ after each stage.

To sum up, token abstraction totally reduces the number of tokens by a factor of $4^3 = 64$ and increases the dimension by a factor of $2^3 = 8$. It structures each frame into a few instance tokens on the basis of selective attention and token agglomeration, which reduces the visual redundancy and also enjoys the advantage of Transformer with an affordable computational costs.

3.3 Token Linking

Assuming that after token abstraction, each frame is structured as J instance tokens. Then a video clip of T frames can be denoted as $\mathcal{Z}_{\text{ins}} = \{\mathbf{z}_t^j | j = 1, 2, ..., J; t = 1, 2, ..., T\}$, where $\mathbf{z}_t^j$ refers to the j-th token in the t-th frame. Here, a sine-based 1D temporal position encoding is additionally added to $\mathcal{Z}_{\text{ins}}$.

The goal of token linking is to link T instance tokens with the same semantic across T frames, so that a video clip can be structurized as J spatiotemporal tubelet tokens. To this end, we propose an exemplar based between-frame one-to-one matching strategy. We first chose $\mathcal{Z}_q = \{\mathbf{z}_r^{j_q} | j_q = 1, 2, ..., J\}$ as the exemplar frame, where $r = \lfloor \frac{T}{2} \rfloor$ is the index of the middle frame in the video clip. We denote the tokens in the exemplar frame and those in rest frames $\mathcal{Z}_k = \{\mathbf{z}_t^{j_k} | \mathbf{z}_t^{j_k} \in \mathcal{Z}_{\text{ins}}, t \neq r\}$ as *query* tokens and *key* tokens, respectively. Then, we compute a similarity matrix $\mathbf{A}$ between the query tokens and the key tokens via a `Gumbel-Softmax` [17] operation computed over the query tokens as

$$\mathbf{A}_t^{(j_q, j_k)} = \frac{\exp(W_q^{j_q} \mathbf{z}_r^{j_q} \cdot W_k^{j_k} \mathbf{z}_t^{j_k} + \gamma_q)}{\sum_{j=1}^{J} \exp(W_q^{j} \mathbf{z}_r^{j} \cdot W_k^{j_k} \mathbf{z}_t^{j_k} + \gamma_j)} \quad s.t. \;\; t \neq r, \tag{9}$$

where $W_q^{j_q}$ and $W_k^{j_k}$ are the weights of the learned linear projections for the j_q-th query tokens and the j_k-th key tokens, respectively, and γs are *i.i.d* random samples drawn from the `Gumbel(0,1)` distribution that enables the `Gumbel-Softmax` distribution to be close with the real categorical distribution. Then, we introduce a modified `nms-one-hot` operation to determine the one-to-one correspondence between the query tokens and the key tokens of each frame. Specifically, for j_k-th key token $\mathbf{z}_t^{j_k}$ in t-th frame, the norm `one-hot` assignment is performed by taking the value of $\texttt{argmax}\{\mathbf{A}_t^{(j_q, j_k)} | j_q = 1, 2, ..., J\}$. However, such an operation cannot ensure a one-to-one correspondence, *i.e.*, more than one key tokens in the same frame could be assigned to the same query token. To address this issue, in `nms-one-hot` scheme, for example, when m_1-th and m_2-th key token in t-th frame are assigned to j_q-th query token simultaneously, we assign the one with a higher similarity, *i.e.*, $\texttt{max}(\mathbf{A}_t^{(j_q, m_1)}, \mathbf{A}_t^{(j_q, m_2)})$, to the j_q-th query token. Then, if $\mathbf{z}_t^{m_1}$ has been assigned to the j_q-th query token, we manually set $\mathbf{A}_t^{(j_q, m_2)}$ as 0 and continue to conduct the assignment operation. Since the `nms-one-hot` operation is not differentiable, we adopt the straight through strategy in [8] to compute the assignment matrix:

$$\hat{\mathbf{A}} = \texttt{nms-one-hot}(\mathbf{A}) + \mathbf{A} - \texttt{sg}(\mathbf{A}), \tag{10}$$

where $\texttt{sg}(\cdot)$ is the stop gradient operator. $\hat{\mathbf{A}}$ is numerically equal to `nms-one-hot` assignments and its gradient is equal to the gradient of $\mathbf{A}$, which makes the token linking module differentiable and end-to-end trainable. Finally, we link the tokens corresponding to the same query token to form the tubelet tokens $\mathcal{Z}_{\text{tube}} = \{\mathbf{z}_{\text{tube}}^j | j = 1, 2, ..., J\}$, which is computed as

$$\mathbf{z}_{\text{tube}}^j = \mathbf{z}_r^j + W_o \frac{\sum_{t=1}^{T} \hat{\mathbf{A}}_t^{(j, \phi(j,t))} W_v \mathbf{z}_t^{\phi(j,t)}}{\sum_{t=1}^{T} \hat{\mathbf{A}}_t^{(j, \phi(j,t))}} \quad s.t. \quad t \neq r, \tag{11}$$

where W_o and W_v are the learned weights of projectors, and $\phi(j, t)$ is the index of token in t-th frame and being assigned to j-th query token.

3.4 Global Context Refining

After token agglomeration and linking, a spatiotemporal video representation is structurized as a few tubelet tokens. On this basis, we perform an additional global attention layer to model global contextual information. Our intuition is two-fold: 1) Global context can significantly boost the performance of interaction recognition, *e.g.*, if grassland is detected, a person is more likely to be playing soccer than basketball. 2) Different interactions can be co-occurring, *e.g.*, a person is `holding` a fork could be `eating` something.

3.5 Decoder & Prediction Head

Decoder. Following the standard architecture in [2], the decoder transforms N_q embeddings by stacking 6 layers consisting of self-attention and cross-attention mechanisms. These embeddings are learned position encodings which are initialized to constants and we refer them to as HOI *queries*. Being added to the input of each attention layer, the N_q queries are transformed as output embeddings by the decoder, which performs global reasoning by using the entire video clip as context.

Prediction head. Following [37], the prediction head is composed of four feed-forward networks (FFNs): human-bounding-box FFNsf_h, object-bounding-box FFNs f_o, object-class FFNs f_o^c, and

action-class FFNs f_a^c. Specifically, f_h and f_o are both a 3-layer perceptron followed by a sigmoid function, which output normalized human- and object-bounding box $\hat{\mathbf{b}}_h \in [0,1]^4$, $\hat{\mathbf{b}}_o \in [0,1]^4$, respectively. f_o^c is a linear layer followed by a softmax function, predicting the probability of object classes $\hat{\mathbf{c}}_o \in [0,1]^{N_{obj}+1}$, where N_{obj} is the number of object classes and the $(N_{obj}+1)$-th element in $\hat{\mathbf{c}}_o$ indicates the query has no corresponding human-object pair. Since actions could be co-occurring, f_a^c is a linear layer followed by a sigmoid function rather than the softmax function. It outputs the probability of action classes $\hat{\mathbf{c}}_a \in [0,1]^{N_{act}}$, which has no an additional element to indicate *no-action*. Here, N_{act} is the number of action classes.

3.6 Loss Function

We follow the loss calculation scheme in [37], including bipartite matching and loss calculation. We describe the detailed calculating process in supplementary material.

4 Experiments

4.1 Datasets & Metrics

We conduct experiments on VidHOI [5] and CAD-120 [22] benchmarks to evaluate the proposed methods by following the standard scheme. VidHOI is a large-scale dataset for V-HOI detection, comprising 6,366 videos for training and 756 videos for validation. In VidHOI, 50 relation categories are annotated, of which half are time-related ones. Mean `AP` (`mAP`) is calculated as the evaluation metric for VidHOI, which is reported over three sets: 1) Full: all 557 categories are evaluated; 2) Rare:315 categories with less than 25 instances and 3) Non-rare: 242 categories with more than 25 instances. CAD-120 is a relatively smaller dataset that consists of 120 RGB-D videos. Here, we only use the RGB images and the 2D bounding boxes annotations of humans and objects. Following standard scheme, we calculate the sub-activity `F1` score as metrics.

4.2 Implementation Details

The dimension of HOI *query* is set to 256, which is the same as the tubelet tokens (32×2^3). The number of queries is set to 100 for VidHOI and 50 for CAD-120. To save computational resources, the backbone is initialized by the backbone weights of QPIC [37], and then frozen without being updated. We employed an AdamW [31] optimizer for 150 epochs. A batch size of 16 on 8 RTX-2080Ti GPUs, and learning rate $l_r = 2.5e^{-4}$ for Transformer and $1e^{-5}$ for FPN are used. The l_r decayed by half at 50-th, 90-th and 120-th epoch, respectively. We use a $l_r = 10^{-6}$ to warm up the training for the first 5 epochs, and then go back to $2.5e^{-4}$ and continue training.

4.3 Analysis of CNN-based & Transformer-based Methods

We compare CNN-based and Transformer-based methods in terms of: 1) long-range dependency modeling, 2) robustness to time discontinuity and 3) contextual relation reasoning.

Long-range dependency modeling. We split HOI instances into bins of size 0.1 according to the normalized spatial distances, and report the APs of each bin. As shown in Figure 3a, our Transformer-based method outperforms existing CNN-based methods in all cases, which becomes increasingly evident as the spatial distance grows. It indicates that Transformer has better long-range dependency modeling capability compared to CNN-based methods that relay on limited receptive field. With this ability, Transformer can dynamically aggregate important information from global context.

Robustness to time discontinuity. we randomly sample one frame every t seconds from the original video to generate a new video as inputs, and report the relative performance compared to the baseline (sampling 1 frame per second). As shown in Figure 3b, the performance of CNN-based methods drop dramatically in contrast to Transformer. The main reason is that the ROI features from different frames are likely to be inconsistent due to the discontinuity of temporal domain. For Transformer, it can be partly solved by learning a variable attention weights to selectively process different features of different frames.

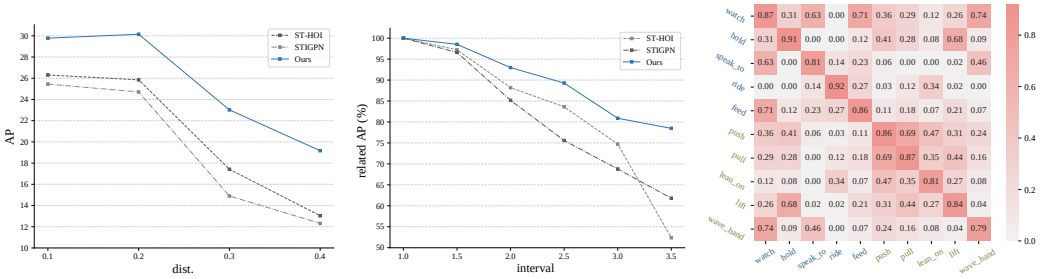

(a) **Spatial distance**. (b) **Temporal pooling**. (c) **Similarity matrix**.

Figure 3: The performance of CNN-based and Transformer-based methods under different scenarios.

Contextual relations reasoning. we randomly pick 5 static interaction types (represented in blue) and 5 dynamic ones (green), each with over 10,000 images. Then, we calculate the average weights of self-attention in the last decoder layer on all pictures where two interactions are co-predicted. As shown in Figure 3c, Transformer can mine the interrelations among different HOI instances, *e.g.*, watch and feed, which two are likely to co-occur, get a relatively high attention weights (0.71).

4.4 Analysis of Token abstraction and Linking

Token abstraction. Table. 1a shows the influence of token abstraction, which is proposed to capture instance level representation. In comparison, CNN-based methods process cropped proposal features (Figure 1(a)), which suffers from temporal inconsistencies and the lack of contextual information, leading to the worst performance. In terms of Transformer, performance is significantly improved (over 25%), but varies under different strategies. Interestingly, adding a simple token fusion module to ViT-like framework (ViT-like†), *i.e.*, fusing every 4 neighboring patch tokens after each Transformer layer, can achieve a 4% relative mAP improvement. It implies that visual redundancy is an obstacle for Transformer to achieve better performance. Moreover, our irregular-window-based (IR-win) token abstraction mechanism achieves the optimal performance. Nevertheless, when replacing all irregular windows in TUTOR with regular windows (R-win), the performance is unexpectedly surpassed by ViT-like†. It indicates that regular windows can reduce the computational complexity, but cannot eliminate visual redundancy thoroughly.

Token linking. Table. 1b shows the influence of token linking. Here, the inputs for all methods are identical, which are the instance tokens generated by token abstraction module. Although computing global attentions along temporal domain without token linking achieves a competitive performance in the detection of time-related interactions, its performance is relatively poor for detecting static HOIs. We conjecture that the instance tokens in different frames are semantically similar, which introduces redundant information to static interaction detection. Moreover, the mAP decreases severely when directly use the value of `Gumbel-Softmax` as assignment weights, *i.e.*, replace the $\hat{\mathbf{A}}$ in Eq.11 with $\mathbf{A}$ in Eq.9. One possible reason is the redundancy arises within token representation due to the absence of zero value in $\mathbf{A}$. In contrast, one-hot assignment is sparse but cannot ensure an one-to-one assignment among frames, which can also cause ambiguity. In comparison, nms-one-hot assignment enforces every T tokens (one per frame) to be linked, which minimizes the ambiguity and redundancy in token representation, thus achieving the optimal performance. We further investigate the effect of video length on these two assignment approaches. As shown in Figure 1c, one-hot assignment surpasses nms-one-hot when a video is longer than 16 seconds, which is caused by the simple way of choosing exemplar frame, *i.e.*, intuitively selecting the middle frame. When a video clip is long, the middle frame is semantically inconsistent with the frames that are temporally far away. We solve this problem by splitting a long video into uniform short clips and performing nms-one-hot assignment in each clip (nms-one-hot*) respectively, which yet introduces more computation.

4.5 Analysis of Effectiveness and Efficiency

Effectiveness. We verify TUTOR's effectiveness of capturing spatial and temporal semantic by observing the performance of detecting static HOI and dynamic HOI when using a quite simple

method	S	T
Proposal	22.84	16.34
ViT-like	27.64	17.30
ViT-like†	28.45	18.64
R-win	28.17	18.24
IR-win	**32.21**	**21.28**

(a) **Token abstraction**.

method	S	T
global	30.07	19.58
gumbel-softmax	28.81	18.11
one-hot	30.64	19.27
nms-one-hot	**32.21**	**21.28**

(b) **Token linking**.

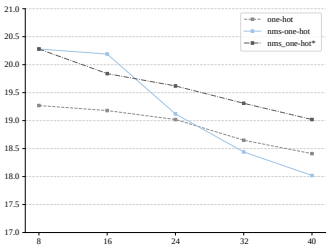

(c) **Tokenization vs. video length**.

Table 1: **Analysis on token abstraction and linking.** We report mAP on detecting dynamic temporal-related (T) and static spatial-related (S) HOI, respectively. ViT-like† in (a) denotes that a regular-window-based token fusing is performed after each Transformer layer. Nms-one-hot* in (c) means to split a long video into several uniform short clips. Default settings are marked in gray.

	case	mAP
spatial	w/ `TA`	**16.42**
	w/o `TA`	9.67
temporal	w/ `TL`	**8.28**
	w/o `TL`	2.30

(a) **Effectiveness**.

case	params	mAP	TFLOPs	FPS	speedup
global	243M	23.51	0.81	0.5	-
w/ `TA`	104M	25.63	0.42	1.2	2×
w/ `TL`	187M	24.28	0.76	0.8	-
w/ `(TA+TL)`	**82M**	**26.84**	**0.25**	**2.0**	4×

(b) **Efficiency**.

Table 2: **Analysis on effectiveness and efficiency.** `TA` is short for token agglomeration and `TL` for token linking. We use clips of size $8 \times 384 \times 384$, with frames sampled at a rate of 1/32.

decoder. For former, we use a 1-layer Transformer decoder on patch tokens in ViT-like method and instance tokens in TUTOR, respectively. the mAP is reported only on static HOI detection. As the Table 2a shows, instance tokens generated by token abstraction can stupendously improve the performance by 70%, compared with patch tokens. It demonstrates that token abstraction mechanism can significantly extract highly-abstracted instance level semantic, which can be easily captured even the decoder is simple. For dynamic HOI detection, we use a 4-layer perception with RELU in between as decoder. Next, we perform a global average pooling on tubelet tokens and instance tokens, which are then fed to the simple decoder to predict the dynamic interactions, respectively. Interestingly, tubelet tokens generated by token linking boost performance by $4\times$, showing us the importance to reduce the temporal redundancy.

Efficiency. Computing attention weights accounts for most of computational overhead in Transformer. Compared to the quadratic computational costs in global attention, we achieve a linear one. As shown in Table 2b, TUTOR achieves a $4\times$ speedup, greatly improving its usability in practical applications. Here, "FPS" is reported in terms of video, *i.e.*, the number of videos being processed per second.

4.6 Ablation Study

Token agglomeration. Token agglomeration is proposed to distill the token representation by selectively merging and projecting the semantically related tokens. We first intuitively try the k-mean [32], an excellent classical clustering algorithm, but obtain a unexpectedly poor performance, as shown in Table 3a. The reason is two-fold:1) it is difficult to integrate the k-mean with the main network into an end-to-end pipeline; 2) it is hard to determine the value of K. Then we replace irregular winodws in TUTOR with regular windows to merge every 4 neighboring tokens, an average pooling operation essentially, which reduces the feature redundancy to some extent. In comparison, irregular-window is more of an operation to selectively merge the semantically similar tokens to model highly abstracted features. It is worth emphasizing that gradually increase the dimension of agglomerated token is interestingly important, which achieves a gain of more than 6% on mAP. We guess that the features are richer with increasing dimensions, as extensively adopted in CNNs.

Window size. Table 3b varies the window size. The instances in an image could have variant sizes. Therefore, a small-sized window is hard to overlap different instances while a large-sized one could cause information mixture as unrelated tokens may be included. We find 7 to be optimal.

Small tricks. We represent some small tricks for key module design in Table 3c. For `nms-one-hot` assignment, another commonly used strategy for merging assigned tokens is to concatenate them and

method	S	T
k-mean	26.71	17.56
r-win	28.82	18.95
ir-win-C	29.34	19.43
ir-win-2C	**32.21**	**21.28**

(a) **Token agglomeration**.

size	S	T
3	24.80	17.92
5	30.69	19.75
7	**32.21**	**21.28**
11	30.28	19.71

(b) **Window size**.

component	trick	S	T
nms-one-hot	concat.	**32.85**	**21.44**
	w-sum	32.21	21.28
p-encoding	3D	31.62	20.59
	(2+1)D	**32.21**	**21.28**
GCR	w/o	31.41	20.63
	w/	**32.21**	**21.28**

(c) **Small tricks**.

Table 3: **Ablation study**. In (a), "nC" is the dimension of agglomerated token. in (c), "p-encoding" is short for position encoding, "w-sum" for weighted-sum, "GCR" for global context refining.

method	backbone	P	VidHOI Full	Rare	NoneRare	S	T	CAD-120 sub-activity(%)
CNN-based methods								
PMF [40] w/ SlowFast	SlowFast [9]	✓	16.31	14.28	23.86	21.77	8.42	-
GPNN [35]	ResNet-101		18.47	16.41	24.50	26.41	16.06	88.9
STIGPN [42]	ResNet-50		19.39	18.22	28.13	26.58	18.46	91.9
ST-HOI [5]	SlowFast	✓	17.60	17.30	27.20	25.00	14.40	-
Transformer-based methods								
HOTR* [20]	ResNet-50		21.14	19.83	30.75	28.36	9.81	-
QPIC* [37]	ResNet-50		21.40	20.56	32.90	28.87	9.74	-
HOTR w/ SlowFast	SlowFast		22.84	21.15	32.86	27.12	13.29	90.7
QPIC w/ SlowFast	SlowFast		22.92	21.64	33.43	28.41	13.47	91.3
TimeSformer [1] w/ decoder	TimeSformer		23.17	21.79	34.57	27.84	18.90	92.5
ours	ResNet-50		**26.92**	**23.49**	**37.12**	**32.21**	**21.28**	**94.7**

Table 4: **comparison with state-of-the-art.** P means human poses, * denotes image-based method.

then project them with a fully-connected layer. Compared with weighted-sum, it can slightly improve performance, but introduces more computation. For position encoding, we factorize the normally used 3D position encoding for spatiotemporal Transformer into a 2D spatial position encoding and a 1D temporal one, which two are added in token agglomeration and linking module, respectively. It is an experiential operation since spatial and temporal information are separately extracted. Global context refining, which refines global contextual information, can achieve almost 1 point gain.

4.7 Comparison with State-of-the-art

Unlike the popularity of image-based HOI detection, relatively less works investigate video-based one as a more practical yet challenging problem. Interestingly, the ability of image-based methods to detect dynamic HOI can be partly improved by replacing the original 2D backbone with a 3D one, but it weaken the ability of detecting static HOIs. With aforementioned strategies, our methods outperforms existing sota methods by a large margins. It is our belief that detecting HOI from video is more reasonable and practical since most interactions are time-related. Therefore, we hope our work will be useful for video-based human activity understanding research.

5 Discussion & Conclusion

Limitation. Our Transformer-based method suffers from the problem of overfitting when handling with small-scale datasets. In our experiments, we have to use the pertrained weights on VidHOI to initialize the model for CAD-120 (small scale), or performance would be severely degraded.
Broader impacts. We know some applications that illegally analyze user behavior by video monitoring. Therefore, strict ethical review is essential to avoid our model being used for such applications.
Conclusion. In this paper, we present TUTOR, a novel spatiotemporal Transformer for video-based HOI detection, which structurizes a video into a few tubelet tokens. To generate compact and expressive tubelet tokens, we propose a token abstraction scheme built on selective attention and token agglomeration, along with token linking strategy to link semantically-related tokens across frames. Our methods outperforms existing works by large margins. Going further, visual redundancy is one of the biggest obstacles for vision Transformer to achieve the same excellent performance as language Transformer, and we will devote more exploration on this in the future works.

References

[1] Gedas Bertasius, Heng Wang, and Lorenzo Torresani. Is space-time attention all you need for video understanding. In *ICML*, 2021. 9

[2] Nicolas Carion, Francisco Massa, Gabriel Synnaeve, Nicolas Usunier, Alexander Kirillov, and Sergey Zagoruyko. End-to-end object detection with transformers. In *ECCV*, 2020. 5

[3] Yu-Wei Chao, Yunfan Liu, Xieyang Liu, Huayi Zeng, and Jia Deng. Learning to detect human-object interactions. In *WACV*, 2018. 2

[4] Mingfei Chen, Yue Liao, Si Liu, Zhiyuan Chen, Fei Wang, and Chen Qian. Reformulating hoi detection as adaptive set prediction. In *CVPR*, 2021. 2

[5] Meng-Jiun Chiou, Chun-Yu Liao, Li-Wei Wang, Roger Zimmermann, and Jiashi Feng. St-hoi: A spatial-temporal baseline for human-object interaction detection in videos. In *ICDAR*, pages 9–17, 2021. 2, 6, 9

[6] Jifeng Dai, Haozhi Qi, Yuwen Xiong, Yi Li, Guodong Zhang, Han Hu, and Yichen Wei. Deformable convolutional networks. In *ICCV*, 2017. 4

[7] Alexey Dosovitskiy, Lucas Beyer, Alexander Kolesnikov, Dirk Weissenborn, Xiaohua Zhai, Thomas Unterthiner, Mostafa Dehghani, Matthias Minderer, Georg Heigold, Sylvain Gelly, et al. An image is worth 16x16 words: Transformers for image recognition at scale. In *ICLR*, 2021. 1, 2

[8] Patrick Esser, Robin Rombach, and Bjorn Ommer. Taming transformers for high-resolution image synthesis. In *CVPR*, pages 12873–12883, 2021. 5

[9] Christoph Feichtenhofer, Haoqi Fan, Jitendra Malik, and Kaiming He. Slowfast networks for video recognition. In *CVPR*, 2019. 9

[10] Chen Gao, Jiarui Xu, Yuliang Zou, and Jia-Bin Huang. Drg: Dual relation graph for human-object interaction detection. In *ECCV*, 2020. 2

[11] Chen Gao, Yuliang Zou, and Jia-Bin Huang. ican: Instance-centric attention network for human-object interaction detection. In *BMVC*, 2018. 2

[12] Noa Garcia and Yuta Nakashima. Knowledge-based video question answering with unsupervised scene descriptions. In *ECCV*, pages 581–598, 2020. 2

[13] Georgia Gkioxari, Ross Girshick, Piotr Dollár, and Kaiming He. Detecting and recognizing human-object interactions. In *CVPR*, 2018. 2

[14] Tanmay Gupta, Alexander Schwing, and Derek Hoiem. No-frills human-object interaction detection: Factorization, layout encodings, and training techniques. In *ICCV*, 2019. 2

[15] Kaiming He, Xiangyu Zhang, Shaoqing Ren, and Jian Sun. Deep residual learning for image recognition. In *CVPR*, 2016. 3

[16] Zhi Hou, Xiaojiang Peng, Yu Qiao, and Dacheng Tao. Visual compositional learning for human-object interaction detection. In *ECCV*, 2020. 2

[17] Eric Jang, Shixiang Gu, and Ben Poole. Categorical reparameterization with gumbel-softmax. In *ICLR*, 2017. 5

[18] Jingwei Ji, Rishi Desai, and Juan Carlos Niebles. Detecting human-object relationships in videos. In *ICCV*, pages 8106–8116, 2021. 2

[19] Bumsoo Kim, Taeho Choi, Jaewoo Kang, and Hyunwoo J. Kim. UnionDet: Union-level detector towards real-time human-object interaction detection. In *ECCV*, 2020. 2

[20] Bumsoo Kim, Junhyun Lee, Jaewoo Kang, Eun-Sol Kim, and Hyunwoo J Kim. Hotr: End-to-end human-object interaction detection with transformers. In *CVPR*, 2021. 2, 9

[21] Dong-Jin Kim, Xiao Sun, Jinsoo Choi, Stephen Lin, and In So Kweon. Detecting human-object interactions with action co-occurrence priors. In *ECCV*, 2020. 2

[22] Hema Swetha Koppula, Rudhir Gupta, and Ashutosh Saxena. Learning human activities and object affordances from rgb-d videos. *IJRR*, pages 951–970, 2013. 2, 6

[23] Yong-Lu Li, Xinpeng Liu, Han Lu, Shiyi Wang, Junqi Liu, Jiefeng Li, and Cewu Lu. Detailed 2d-3d joint representation for human-object interaction. In *CVPR*, 2020. 2

[24] Yong-Lu Li, Siyuan Zhou, Xijie Huang, Liang Xu, Ze Ma, Hao-Shu Fang, Yanfeng Wang, and Cewu Lu. Transferable interactiveness knowledge for human-object interaction detection. In *CVPR*, 2019. 2

[25] Jingyun Liang, Jiezhang Cao, Yuchen Fan, Kai Zhang, Rakesh Ranjan, Yawei Li, Radu Timofte, and Luc Van Gool. Vrt: A video restoration transformer. *arXiv preprint arXiv:2201.12288*, 2022. 2

[26] Tsung-Yi Lin, Piotr Dollár, Ross Girshick, Kaiming He, Bharath Hariharan, and Serge Belongie. Feature pyramid networks for object detection. In *CVPR*, 2017. 3

[27] Xue Lin, Qi Zou, and Xixia Xu. Action-guided attention mining and relation reasoning network for human-object interaction detection. In *IJCAI*, 2020. 2

[28] Xiaolong Liu, Qimeng Wang, Yao Hu, Xu Tang, Song Bai, and Xiang Bai. End-to-end temporal action detection with transformer. *arXiv preprint arXiv:2106.10271*, 2021. 2

[29] Yang Liu, Qingchao Chen, and Andrew Zisserman. Amplifying key cues for human-object-interaction detection. In *ECCV*, 2020. 2

[30] Ze Liu, Yutong Lin, Yue Cao, Han Hu, Yixuan Wei, Zheng Zhang, Stephen Lin, and Baining Guo. Swin transformer: Hierarchical vision transformer using shifted windows. In *ICCV*, 2021. 3

[31] Ilya Loshchilov and Frank Hutter. Decoupled weight decay regularization. 2017. 6

[32] James MacQueen et al. Some methods for classification and analysis of multivariate observations. In *Proceedings of the fifth Berkeley symposium on mathematical statistics and probability*, 1967. 8

[33] Tushar Nagarajan, Christoph Feichtenhofer, and Kristen Grauman. Grounded human-object interaction hotspots from video. In *ICCV*, pages 8688–8697, 2019. 2

[34] Megha Nawhal, Mengyao Zhai, Andreas Lehrmann, Leonid Sigal, and Greg Mori. Generating videos of zero-shot compositions of actions and objects. In *ECCV*, pages 382–401, 2020. 2

[35] Siyuan Qi, Wenguan Wang, Baoxiong Jia, Jianbing Shen, and Song-Chun Zhu. Learning human-object interactions by graph parsing neural networks. In *ECCV*, 2018. 2, 9

[36] Sai Praneeth Reddy Sunkesula, Rishabh Dabral, and Ganesh Ramakrishnan. Lighten: Learning interactions with graph and hierarchical temporal networks for hoi in videos. In *ACMMM*, pages 691–699, 2020. 2

[37] Masato Tamura, Hiroki Ohashi, and Tomoaki Yoshinaga. Qpic: Query-based pairwise human-object interaction detection with image-wide contextual information. In *CVPR*, 2021. 2, 5, 6, 9

[38] Oytun Ulutan, ASM Iftekhar, and Bangalore S Manjunath. Vsgnet: Spatial attention network for detecting human object interactions using graph convolutions. In *CVPR*, 2020. 2

[39] Ashish Vaswani, Noam Shazeer, Niki Parmar, Jakob Uszkoreit, Llion Jones, Aidan N Gomez, Łukasz Kaiser, and Illia Polosukhin. Attention is all you need. In *NIPS*, 2017. 2

[40] Bo Wan, Desen Zhou, Yongfei Liu, Rongjie Li, and Xuming He. Pose-aware multi-level feature network for human object interaction detection. In *ICCV*, 2019. 2, 9

[41] Hai Wang, Wei-shi Zheng, and Ling Yingbiao. Contextual heterogeneous graph network for human-object interaction detection. In *ECCV*, 2020. 2

[42] Ning Wang, Guangming Zhu, Liang Zhang, Peiyi Shen, Hongsheng Li, and Cong Hua. Spatio-temporal interaction graph parsing networks for human-object interaction recognition. In *ACMMM*, pages 4985–4993, 2021. 2, 9

[43] Tiancai Wang, Rao Muhammad Anwer, Muhammad Haris Khan, Fahad Shahbaz Khan, Yanwei Pang, Ling Shao, and Jorma Laaksonen. Deep contextual attention for human-object interaction detection. In *ICCV*, 2019. 2

[44] Yuqing Wang, Zhaoliang Xu, Xinlong Wang, Chunhua Shen, Baoshan Cheng, Hao Shen, and Huaxia Xia. End-to-end video instance segmentation with transformers. In *CVPR*, pages 8741–8750, 2021. 2

[45] Bingjie Xu, Junnan Li, Yongkang Wong, Qi Zhao, and Mohan S Kankanhalli. Interact as you intend: Intention-driven human-object interaction detection. *TMM*, 2019. 2

[46] Dongming Yang and Yuexian Zou. A graph-based interactive reasoning for human-object interaction detection. *IJCAI*, 2020. 2

[47] Aixi Zhang, Yue Liao, Si Liu, Miao Lu, Yongliang Wang, Chen Gao, and Xiaobo Li. Mining the benefits of two-stage and one-stage hoi detection. *NIPs*, 34, 2021. 2

[48] Chenlin Zhang, Jianxin Wu, and Yin Li. Actionformer: Localizing moments of actions with transformers. *arXiv preprint arXiv:2202.07925*, 2022. 2

[49] Xubin Zhong, Changxing Ding, Xian Qu, and Dacheng Tao. Polysemy deciphering network for robust human–object interaction detection. In *ICCV*, 2021. 2

[50] Penghao Zhou and Mingmin Chi. Relation parsing neural network for human-object interaction detection. In *ICCV*, 2019. 2

[51] Tianfei Zhou, Wenguan Wang, Siyuan Qi, Haibin Ling, and Jianbing Shen. Cascaded human-object interaction recognition. In *CVPR*, 2020. 2

[52] Xizhou Zhu, Weijie Su, Lewei Lu, Bin Li, Xiaogang Wang, and Jifeng Dai. Deformable detr: Deformable transformers for end-to-end object detection. In *ICLR*, 2021. 4

[53] Cheng Zou, Bohan Wang, Yue Hu, Junqi Liu, Qian Wu, Yu Zhao, Boxun Li, Chenguang Zhang, Chi Zhang, and Yichen Wei. End-to-end human object interaction detection with hoi transformer. In *CVPR*, 2021. 2

Checklist

The checklist follows the references. Please read the checklist guidelines carefully for information on how to answer these questions. For each question, change the default **[TODO]** to [Yes] , [No] , or [N/A] . You are strongly encouraged to include a **justification to your answer**, either by referencing the appropriate section of your paper or providing a brief inline description. For example:

- Did you include the license to the code and datasets? [Yes]
- Did you include the license to the code and datasets? [No] The code and the data are proprietary.
- Did you include the license to the code and datasets? [N/A]

Please do not modify the questions and only use the provided macros for your answers. Note that the Checklist section does not count towards the page limit. In your paper, please delete this instructions block and only keep the Checklist section heading above along with the questions/answers below.

1. For all authors...
   (a) Do the main claims made in the abstract and introduction accurately reflect the paper's contributions and scope? [Yes]
   (b) Did you describe the limitations of your work? [Yes] See Section 5.
   (c) Did you discuss any potential negative societal impacts of your work? [Yes] See Section 5.
   (d) Have you read the ethics review guidelines and ensured that your paper conforms to them? [Yes]
2. If you are including theoretical results...
   (a) Did you state the full set of assumptions of all theoretical results? [N/A]
   (b) Did you include complete proofs of all theoretical results? [N/A]
3. If you ran experiments...
   (a) Did you include the code, data, and instructions needed to reproduce the main experimental results (either in the supplemental material or as a URL)? [Yes] The code is provided in supplementary material.

(b) Did you specify all the training details (e.g., data splits, hyperparameters, how they were chosen)? [Yes]

(c) Did you report error bars (e.g., with respect to the random seed after running experiments multiple times)? [No]

(d) Did you include the total amount of compute and the type of resources used (e.g., type of GPUs, internal cluster, or cloud provider)? [Yes]

4. If you are using existing assets (e.g., code, data, models) or curating/releasing new assets...

(a) If your work uses existing assets, did you cite the creators? [Yes]

(b) Did you mention the license of the assets? [No]

(c) Did you include any new assets either in the supplemental material or as a URL? [N/A]

(d) Did you discuss whether and how consent was obtained from people whose data you're using/curating? [N/A]

(e) Did you discuss whether the data you are using/curating contains personally identifiable information or offensive content? [N/A]

5. If you used crowdsourcing or conducted research with human subjects...

(a) Did you include the full text of instructions given to participants and screenshots, if applicable? [N/A]

(b) Did you describe any potential participant risks, with links to Institutional Review Board (IRB) approvals, if applicable? [N/A]

(c) Did you include the estimated hourly wage paid to participants and the total amount spent on participant compensation? [N/A]

A Appendix

Optionally include extra information (complete proofs, additional experiments and plots) in the appendix. This section will often be part of the supplemental material.